sustainability

MDPI

Article

The Use of Superabsorbent Polymers in High Performance Concrete to Mitigate Autogenous Shrinkage in a Large-Scale Demonstrator

Laurence De Meyst [1,†], Judy Kheir [1,2,†], José Roberto Tenório Filho [1], Kim Van Tittelboom [1] and Nele De Belie [1,*]

[1] Magnel-Vandepitte Laboratory for Structural Engineering and Building Materials, Ghent University, Technologiepark Zwijnaarde 60, B-9052 Ghent, Belgium; laurence.demeyst@ugent.be (L.D.M.); judy.kheir@ugent.be (J.K.); roberto.tenorio@ugent.be (J.R.T.F.); kim.vantittelboom@ugent.be (K.V.T.)

[2] Institut de Recherche en Génie Civil et Mécanique (GeM), UMR-CNRS 6183, Ecole Centrale de Nantes, 1 rue de la Noë, 44321 Nantes, France

* Correspondence: nele.debelie@ugent.be; Tel.: +32-9-264-55-22

† These authors have contributed equally to this publication.

Received: 13 May 2020; Accepted: 5 June 2020; Published: 10 June 2020

Abstract: High performance concrete (HPC) is a high strength concrete that undergoes a lot of early-age autogenous shrinkage (AS). If shrinkage is restrained, then micro-cracks arise and threaten the durability of the structure. Superabsorbent polymers (SAPs) can reduce/mitigate the autogenous shrinkage, due to their promising application as internal curing agents. In this paper, large-scale demonstrators were built to investigate the efficiency of SAPs to mitigate autogenous shrinkage in HPC. For this purpose, different measurement techniques were used like embedded fiber optic sensors and demountable mechanical strain gauges, complemented by AS measurements in corrugated tubes and restrained ring tests. The SAP wall showed an AS reduction of 22%, 54%, and 60% at the bottom, middle, and top, respectively, as recorded by the sensors (in comparison with the reference wall (REF)). In the corrugated tubes, mitigation of AS was shown in the SAP mixture, and under restrained conditions, in the ring test, the reference mixture cracked after two days, while the SAP mixture had not cracked at the end of the measurement period (20 days). Cracks were shown on REF wall after one day, while the SAP wall was crack-free. Water flow tests performed on the main crack of the REF wall confirmed that the flow rate is related to the third power of the crack width. All tests showed that SAPs could highly reduce AS in HPC and avoid cracking.

Keywords: high performance concrete; internal curing; superabsorbent polymers; autogenous shrinkage; large-scale testing

1. Introduction

High performance concrete (HPC) is a cementitious material with high compressive strength (>100 MPa), a low permeability and a high durability thanks to its dense matrix [1]. HPC is characterized by a low water to cement (w/c) ratio (typically 0.35 or lower), small maximum aggregate sizes (often smaller than 10 mm) and the presence of fine fillers or supplementary cementitious materials like silica fume for obtaining a dense concrete matrix [2]. However, this type of concrete is very prone to autogenous shrinkage due to the extremely low w/c-ratio, and therefore, the formation of cracks is inevitable. Due to a lack of free water caused by the consumption of water during the cement hydration process, and when no external water source is present, the internal relative humidity (RH) will drop resulting in self-desiccation (RH < 100%) [3,4]. The pore fluid is then subjected to an increasing capillary pressure, and consequently, the skeleton suffers from increasing stresses leading

to autogenous shrinkage. This can result in micro- and macro-cracks which impair the strength, durability and aesthetics of the concrete structure. Also, these cracks can create preferential pathways for water and gasses possibly containing harmful substances which could induce steel corrosion, frost attack, sulphate attack, etc. resulting in a decreased durability and structural integrity of the concrete structure [5].

Shrinkage of cementitious materials is divided into two stages [6,7]: early-age and later-age shrinkage. Early-age shrinkage, i.e., during the first 24 h after mixing, is of great importance since, at that age, the material has not yet gained substantial strength, and hence, resistance against crack formation. This results in micro-cracks which can widen over time due to later-age shrinkage, i.e., beyond 24 h after mixing. The sum of both early-age and later-age or long-term shrinkage is the total shrinkage of the cementitious material [8].

Autogenous shrinkage, which starts right after the contact between water and cement [7], becomes more pronounced after setting and continues as long as hydration takes place. It is a type of shrinkage which could have a negative effect on the cementitious material during the early-age stage. Therefore, mitigating this type of shrinkage is of great importance. One possibility of minimizing and/or mitigating autogenous shrinkage is by internal curing. The basis of this approach is the release of water inside the cementitious matrix during cement hydration when the relative humidity (RH) starts to drop and self-desiccation initiates. There exists a wide variety of curing techniques: both external and internal curing can be applied, and the latter is an upcoming practice since some drawbacks are related to the external curing technique as it cannot be used for the mitigation of autogenous shrinkage. This type of shrinkage occurs over the complete volume and not only at the surface of the cementitious material. Therefore, external curing will not be sufficient to mitigate autogenous shrinkage in (U)HPC since it only cures the cementitious material at the surface, and as stated above, (U)HPC is characterized by a dense microstructure and low permeability which makes it difficult for the curing water to travel longer distances into the matrix [1,9,10]. For internal curing, several materials can be used, such as lightweight aggregates (LWA), pumice, expanded clay or superabsorbent polymers (SAPs) [11]. LWA are very efficient in reducing or even eliminating autogenous shrinkage. However, the use of LWA is also associated with some important disadvantages: (1) The consistency is hard to control [11]; (2) it causes the formation of voids and flaws of which the size and shape cannot be controlled resulting in a broad variety of sizes and shapes. Consequently, a reduction of the flexural strength and Young's modulus is triggered [11]. The use of SAPs in cementitious materials as an internal curing agent is, on the contrary, more favorable as the shape, size and distribution of the voids and flaws can be controlled [12,13].

Superabsorbent polymers are able to absorb up to 500 times their own weight in aqueous solutions, resulting in a swollen hydrogel. At a later stage in time, the SAPs can gradually release their water at the appropriate moment during the hydration process, maintaining the RH and minimizing the self-desiccation. In that way, autogenous shrinkage can be reduced or even mitigated [3,10,12–15]. After the final setting time of the mixture, the relative humidity drops to less than 95% (Figure 1); thus, the water that was absorbed by the SAPs during mixing will be released to compensate for the loss of water that is being used for the cement hydration.

While cement hydration is a process that continues to take place over the service life of the structure, the highest rate of the hydration reaction is found at the early-age stage. The hydration of cement is based on the consumption of water in order to produce hydration products that will act as bridges between the cement grains to further enhance the strength and reduce the porosity. When the water to cement (w/c) ratio of a mix is very low, for instance, less than 0.3 (as it is the case for ultra-high and high performance concrete), cement grains will use the water available and not enough of this water will remain for the inner part of the cement grains that do not have direct access to the aqueous liquid. Therefore, the pressure in the interconnection between these particles, i.e., in the canals or pores between two cement particles, will increasingly try to attract the water into the empty space to reach an equilibrium state. The pores filled with water will start to be emptied due to the exerted pressure from

the empty space to try and reach an equilibrium state. A meniscus will form inside the water-filled pore that is being emptied, and at that point, while the angle of the water meniscus is decreasing, the contact angle (the angle between the tangents of water and particle) will decrease as well. As a result, water pressure will be exerted on the outer face of the hydration products. This pressure is perceived as a tensile force on the outer face of the particle and tends to break the connections between the cement grains formed by the hydration products, and since concrete can only bear limited tensile stresses, cracks start to appear at a very early-age, due to autogenous shrinkage. For that reason, autogenous shrinkage plays an important role in concrete where w/c ratios are very low (Figure 2).

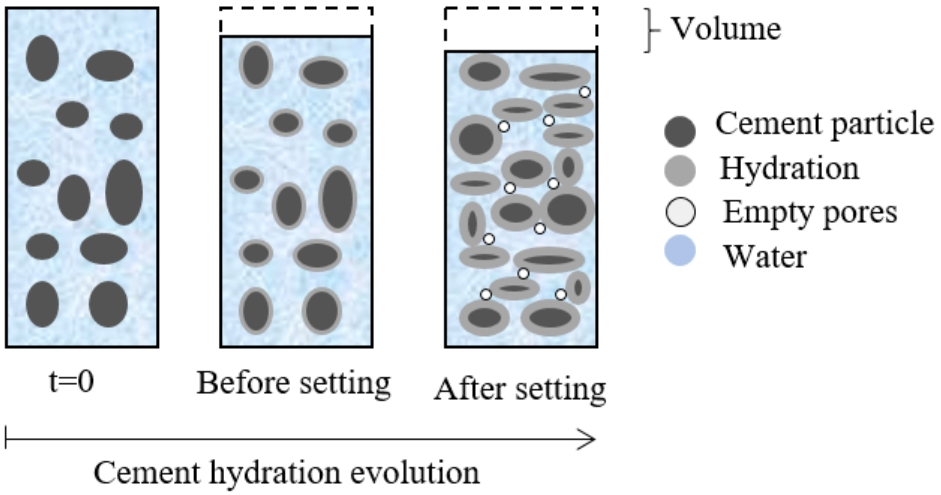

Figure 1. The evolution of the cement hydration over time, adapted from Reference [16].

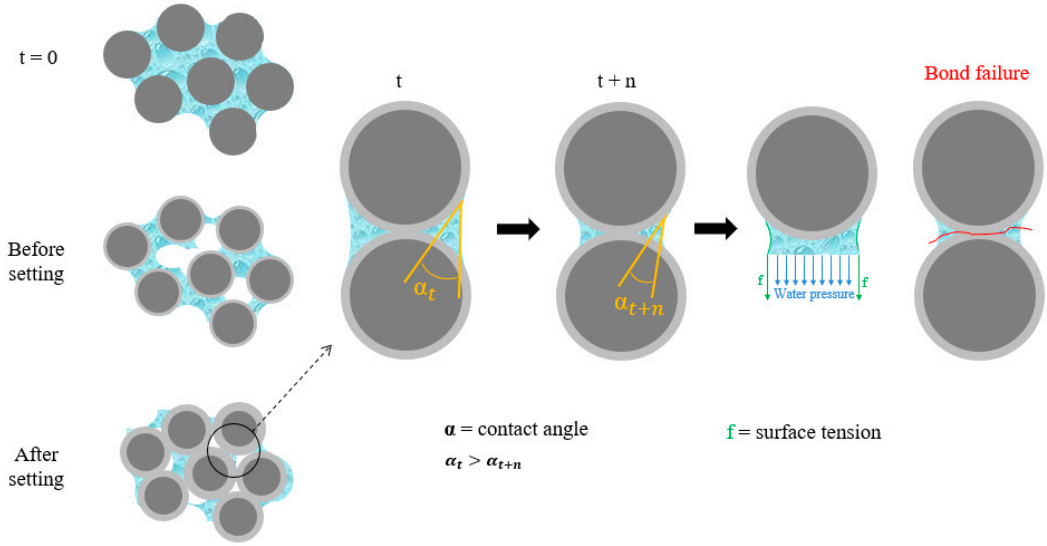

Figure 2. Schematic diagram of the autogenous shrinkage process over time which leads to cracking at the early-age stage.

In the literature, different tests are described to measure (autogenous) shrinkage in mortar or concrete: The restrained ring test according to the American Society of Testing and Materials ASTM C 1581-04 [17], the corrugated tube test according to ASTM C 1698-09 [18], the use of embedded sensors [19–21], the use of demountable mechanical strain gauge (DEMEC) measurements [22,23]. The corrugated tube combines the advantages of linear and volumetric methods while avoiding most of the disadvantages in other methods like loss of moisture, longitudinal restraints, difficulty to start the measurements before hardening, practical difficulties in handling the specimens. Although the corrugated tube test is not applicable for concrete, because of the presence of aggregates, this was

not a problem in this study due to the relatively small aggregate size used. The advantages of using fiber optic sensors lie within the ability to monitor the strain development in concrete structures under different environmental conditions from the moment of casting, which can be of great interest to study the effect of shrinkage in concrete at a very early-age; they also present a higher level of precision and reduced workforce for recording shrinkage measurements, but their high-cost can be a disadvantage [24]. The restrained ring test, which is normally used to evaluate the shrinkage of concrete specimens under restrained conditions, was used in this study as well, to compare the results of both measuring techniques.

Cracking behavior is very important with regard to quality or durability requirements. Crack development in concrete increases its permeability and enhances the flow paths, thus allowing for more water or aggressive chemical agents into the matrix and facilitating the deterioration of the concrete. The degree of the permeability increases with the value of the crack opening in the concrete. [25]. This is an unwanted behavior for HPCs, since users of this specific type of concrete tend to use it for its enhanced durability properties with low permeability and very high strength. Cracking in HPC mainly occurs due to the autogenous and restrained shrinkage.

Very few studies in the literature performed shrinkage tests on large scale HPC elements, for example, Cusson et al. [26] studied the early-age thermo-mechanical behavior of large prismatic HPC specimens (200 mm × 200 mm × 1000 mm) under restrained autogenous shrinkage and realistic temperature conditions. It was discussed how the self-desiccation of these types of concrete was pronounced at the very early-age stage, and considerably increased the risk of cracking, which was estimated to be highest at the age of 1.5 days. Studies performed on a large scale HPC elements with SAPs in the mix to reduce/mitigate cracks induced by AS are almost non-existent, for that reason, and to better understand the behavior of a real structure this study was performed. SAPs being a copolymer of acrylamide and sodium acrylate (particle size 100.0 ± 21.5 µm, n = 100) (BASF (Baden Aniline and Soda Factory), Ludwigshafen, Germany) were embedded in an HPC demonstrator wall. Shrinkage measurements were performed by means of embedded fiber optic sensors and DEMEC measurements and compared to the shrinkage of a reference wall without SAP. The material performance of the HPC mixes with and without SAP was furthermore investigated in ring tests and corrugated tube tests. Water flow tests were also investigated on the crack induced by autogenous shrinkage on the reference wall to see the influence of crack development on the permeability and durability of HPC.

2. Materials and Methods

2.1. The Demonstrator

2.1.1. Slabs

The demonstrator consisted of a wall cast on a slab, see schematic representation in Figure 3. This setup was chosen to restrain the shrinkage at the slab-wall connection in order to create shrinkage cracks at that location.

The slabs had dimensions of 2 m × 0.95 m × 0.2 m (l × w × t) with two reinforcement meshes (150 mm) of diameter 8 mm positioned at a concrete cover of 25 mm. The slab was cast of traditional concrete, with the composition shown in Table 1 and the following mixing procedure was used using a rotating pan mixer Zyklos from the company Pemat (Freisbach, Germany) with a capacity of 200 L (speed of rotation for the mixing blades equal to 46 rpm and 189 rpm for the pan):

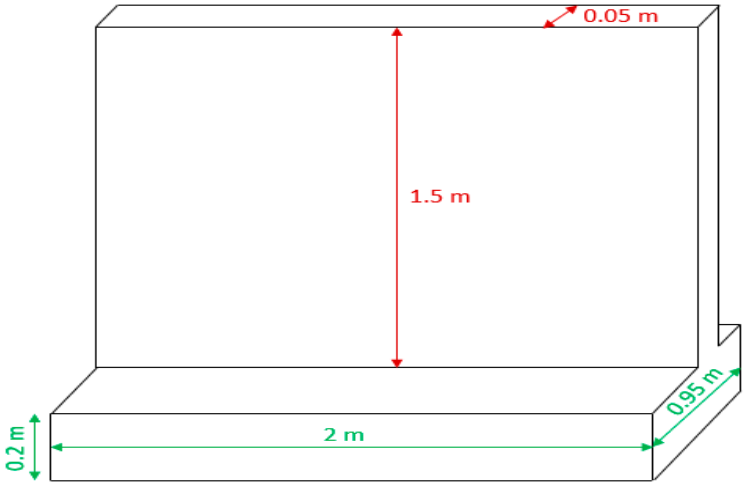

Figure 3. Schematic representation of the restrained wall on the slab.

The slabs were demolded after two days, and were stored at an ambient temperature for four months (ranging between 7 °C to 22 °C) in order to allow the shrinkage and deformation of the slabs in an unrestrained way, then they were moved to a climate-controlled room with a temperature of 20 ± 2 °C and RH 60 ± 5% where the walls were cast on top. In order to restrain the shrinkage of the wall, the slab and wall were connected with a steel mesh (mesh size 10 mm, diameter 2 mm and height of 60 mm) into the wall over the length of the wall and two reinforcement bars with a diameter of 12 mm and the total length of 300 mm at both ends, see Figure 4. Both the mesh and the reinforcement bars were positioned in the slab (by sawing a slot and drilling a hole) and glued with epoxy afterwards; the bars were placed at 75 mm away from the sides of the slab.

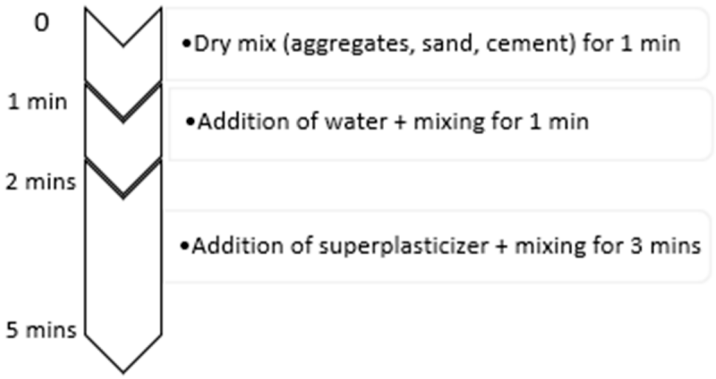

Table 1. Traditional concrete composition for the slab.

Materials	kg/m^3
Sand 0/4	670
Gravel 2/8	490
Gravel 8/16	790
CEM I 52.5 N	300
Water	150
BASF Glenium 27 superplasticizer	1.67

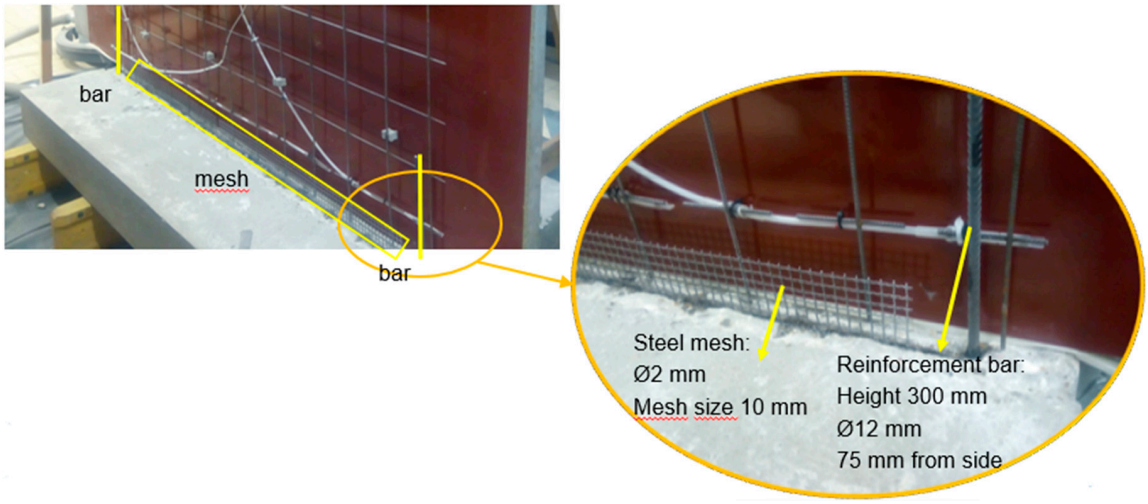

Figure 4. Slab-wall connection.

2.1.2. Walls

Two different walls were cast on top of two separate slabs: One reference wall without SAPs (REF) and one wall with commercial SAPs. The composition of both walls can be found in Table 2.

Table 2. Concrete composition of the reference and the super-absorbent polymers (SAP) walls.

Materials	REF (kg/m^3)	SAP (kg/m^3)
Sand 0/4	401.9	373.9
Basalt 4/8	649.3	604.4
Silica Fume-Elkem Microsilica 940 U	153.8	143.1
Cement-Variodur 40 (CEM III/A 52.5 R)	778.2	723.9
Filler-Betofill VK50	185.5	172.6
Water	186.4	173.4
Superplasticizer-SIKA Viscocrete UHPC-2	8.560 *	8.690 **
SAPs-BASF	-	2.1717 ***
Extra water absorbed by SAP	-	58.6

* 1.1 m% by weight of cement type III/A 52.5 R "Variodur 40" for REF. ** 1.1 m% by weight of Variodur 40 + 0.1 m% extra to maintain workability. *** 0.3 m% SAPs by weight of Variodur 40. SAPs-BASF; Superabsorbent polymers Baden Aniline and Soda Factory.

The commercially available SAP is synthesized by bulk polymerization creating the copolymer poly (acrylamide-co-acrylic acid) out of the monomers acrylamide and sodium acrylate. Due to the fabrication process, the SAPs had an irregular shape. The d_{50} of the SAPs was 100 µm. The other components of the concrete mixture were sand 0/4, basalt 4/8, Microsilica 940 U from the company Elkem with a bulk density between 200–350 kg/m^3, filler Betofill VK50 from the company Franzefoss Minerals and superplasticizer ViscoCrete UHPC-2 from SIKA. The cement "Variodur 40" from the company Dyckerhoff is a CEM III/A 52.5 R, thus contains 35–64% clinker, 36–65% blast furnace slag (BFS) and 0–5% minor additional constituents. It was shown by Snoeck et al. [3] that the replacement of cement with varying amounts of BFS and fly ash (FA) led to less autogenous strain at w/c = 0.3. Therefore, the use of blended cement with BFS will contribute in the reduction of strains induced by AS. Based on preliminary tests by the authors, it was decided to add 0.3 m% SAPs by cement weight. In the case where SAPs are added to the mixture, extra water to compensate for the water uptake by the SAPs is added, based on the swelling capacity (equal to 27 g/g_{SAP}) of the SAPs from a filtration test in the cement slurry (measurement is taken after 10 min absorption) [27]. These SAPs had a swelling capacity of 288 g of demineralized water per gram of SAP after 10 min, 270 g/g_{SAP} after 1 h and

201 g/g_{SAP} after 24 h, in the cement slurry their swelling capacity was equal to 28 g/g_{SAP} after 1 h and 21.5 g/g_{SAP} after 24 h. In order to obtain the same workability as for the reference mixture, an extra amount of 0.1 m% by weight of cement of superplasticizer was added to the mixture used for the SAP wall. Note that the swelling capacities of SAPs in cement filtrate solution are much lower compared to the ones in demineralized water, and that is because the presence of K^+, Na^+, Mg^{2+} or Ca^{2+} cations in cement solution. These cations enhance the creation of the charge screening effect of the negatively charged polymer chains, resulting in a lower repulsion of chains and a lowered fluid absorption and less swelling of the SAP particles. In addition, Ca^{2+} (or any divalent cation) can act as cross-linker which offers an additional reduction of the swelling properties; the higher the cross-linking degree, the lower the swelling capacity [28–30]. The evolution in time of the swelling capacity of SAPs in demineralized water and in cement filtrate for different types of SAPs and concentrations can be found in [31]. Therefore, the decrease in the swelling capacity of the SAPs used in this research at 24 h, could be linked to the additional change in the ion concentration with time of the cement filtrate solution that leads SAPs to be highly cross-linked.

The mixing procedures for the reference wall and the SAP wall, using a rotating pan mixer Zyklos from the company Pemat-Germany with a capacity of 200 L (speed of rotation for the mixing blade equal to 46 rpm and 189 rpm for the pan), were as follows:

Mixing procedure for the reference wall:

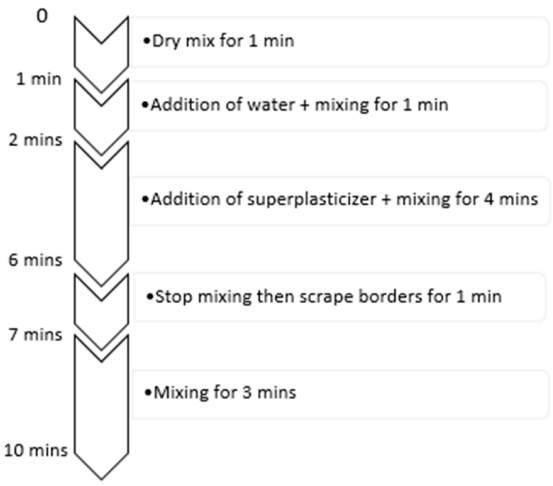

Mixing procedure for the SAP wall:

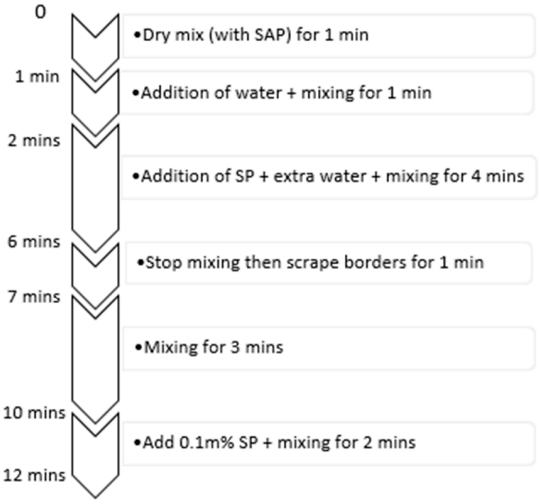

The SAPs were therefore added at once together with the other dry constituents. When using SAPs as internal curing agents, one needs to assure a uniform distribution of the SAPs within the matrix to make sure the water reaches the points where self-desiccation might occur. This is justifiable when considering that the water released from the SAPs can move around a limited distance in the surroundings of the SAPs [32]. If the SAPs would have been presoaked before addition to the mix, the dry SAP particles become a hydrogel that might prove difficult to disperse within the mixture, thus causing agglomeration. The agglomeration can then lead to a non-uniform distribution of water reservoirs and ineffective internal curing. As another possible approach, Tenorio Filho et al. [33] studied the effect of adding the SAPs in the mixture after all the other materials and water had been mixed together and compared the results with a mixture of the same composition where the SAPs had been added together with the dry materials and prior to the addition of water. The results showed a reduction of 32% in the effectiveness of the SAPs for mitigating autogenous shrinkage when added after the water had been mixed with the other materials. An air void analysis showed that the macro-pores formed, due to water release by the SAPs was 2 to 3 times bigger in the system with SAPs added after water, concluding that such approach can indeed lead to agglomeration and ineffective mitigation of autogenous shrinkage.

Due to the use of the SIKA ViscoCrete UHPC-2, the HPC mixture was self-compacting. It was poured into the mold from the top using 3 batches of 90 liters and no further vibration was needed. The time between the first and the third batch was around 40 min. The wall was poured in a time frame of 55 min and kept in a climate-controlled room with a temperature of 20 ± 2 °C and relative humidity (RH) of 60 ± 5%) for the testing period (120 days). The formwork was removed 19 h after water-cement contact for both walls. The fresh and hardened properties of the concrete used to cast the walls will be discussed in the upcoming sections. It should be mentioned that all of the experiments done in this study were performed on the same batches as used for the walls except for the ring tests (restrained shrinkage), for which the same mixture was used, but from a different batch.

The wall had dimensions of 1.5 m × 2 m × 0.05 m (h × l × t) reinforced by a steel mesh (150 mm and diameter 5 mm). The wall was kept thin to limit the heat production of the cement hydration process of the high performance concrete, in order to avoid a too large thermal gradient and subsequent thermal cracking. A picture of both walls is depicted in Figure 5.

Figure 5. Reference wall (REF) (**left**) and super-absorbent polymers (SAP) wall (**right**).

2.2. *Methods*

2.2.1. Hardened Concrete Properties of the Slabs

The compressive strength at 7 and 28 days and E-modulus at 28 days of the slabs were determined on cast cylindrical specimens (height 300 mm and diameter 150 mm) according to NBN EN 12390-3 [34] and NBN EN 12390-13 [35], respectively.

2.2.2. Fresh Concrete Properties of the Walls

The slump flow of the self-compacting concrete was measured according to NBN EN 12350-8 [36], the minimum slump flow value for self-compacting concrete (class SF1) equals 550 mm. The slump flow was determined once for the reference and the SAP mixtures.

To determine the air content of the fresh concrete, the pressure gauge method described in NBN EN 12350-7 [37] was used. The air content was determined once for the reference and the SAP mixtures.

To determine the density of the fresh self-compacting concrete, the method described in NBN EN 12350-6 [38] was followed. The density of the fresh mixture was determined once for the reference and the SAP mixtures.

To determine the time of final setting of the concrete mixtures (which will be later used as the start of the autogenous shrinkage measurements in the corrugated tube test and for fiber opticSurveillance d'Ouvrages par Fibres Optique ()sensors measurements), the penetrometer test according to the

standard ASTM C 403 [39] was executed. Therefore, the mortar was sieved from the fresh concrete and cubes with dimensions of 150 × 150 × 150 mm^3 were filled with this sieved mortar, one cube for each mixture was tested. In between all the penetration measurements, the mold was sealed with plastic foil to exclude the effect of drying and stored in a climate-controlled room of 20 ± 2 °C and 60 ± 5% RH. The final setting time was determined for the reference and the SAP mixtures.

2.2.3. Hardened Concrete Properties of the Walls

The compressive strength of the concrete was measured on three cast cylinders with a height of 300 mm and a diameter of 150 mm, according to NBN EN 12390-3 [34]. The compressive strength was determined experimentally at the age of seven and 85 days for the REF mixture, and seven and 63 days for the SAP mixture. At the age of 28 days, the values were modelled following the strength evolution Equations (1) and (2) according to CEB-FIP Model [40]. At the same ages, the E-modulus was also determined in triplicate on the same cast cylindrical specimens used afterwards for the compressive test (height 300 mm and diameter 150 mm), according to the standard NBN EN 12390-13 [35].

2.2.4. Autogenous Shrinkage with Corrugated Tubes

The autogenous shrinkage was monitored over time for 20 days following the Standard ASTM C 1698 09 [18] to study the effects of internal curing by the SAPs on the autogenous shrinkage properties. Freshly mixed concrete was poured into a corrugated tube with an outer diameter of 29 ± 0.5 mm that offers little resistance to the length change of the specimen. The mold was sealed to prevent moisture loss, and the specimen was stored at a constant temperature of 20 ± 2 °C. The length of the specimen was measured automatically using an LVDT with a measuring range of 5 mm and an accuracy of 2.5 µm. The change in length was recorded every ten minutes until the age of 20 days. The change in length and the original length of the specimen were used to compute the autogenous strain. For each mixture, three tubes were tested. Although most results in the literature are dealing with corrugated tubes filled with mortar ([1,41]) or cement paste ([14,42,43]), the tubes were filled with concrete in this experiment. As the used aggregates were quite small in this concrete type (basalt 4–8 mm), it was possible to fill the tubes with concrete without any problems. Ji et al. [44] measured the AS of the concrete mixture using larger corrugated tubes with an outer diameter of 80 mm, because they had larger coarse aggregates with a diameter bigger than 9 mm. A picture of the test setup is shown in Figure 6.

Figure 6. Autogenous shrinkage corrugated tube setup.

2.2.5. Restrained Shrinkage Measurements with Ring Tests

To measure the restrained shrinkage of concrete, a restrained ring test was performed based on the recommendations in ASTM C 1581-04 [17]. In this test, a steel ring instrumented with three strain gauges was filled with concrete directly after mixing. A schematic overview (left) and a picture (right) of the ring test setup is depicted in Figure 7.

From each mixture, one ring was filled with fresh concrete, and the strain of the specimen was measured at three locations every ten minutes from the time of casting onwards, until the age of 20 days. A sudden change in strain was an indication of cracking of the test specimen. After casting, the bolts (see Figure 7) were loosened, and the rings were sealed with plastic foil. The rings were kept in a climate-controlled room at 20 ± 2 °C and 60 ± 5% relative humidity (RH). After 19 h, the outer steel ring was removed (similar as for the removal of the formwork from the walls), and the rings were again completely wrapped in plastic foil to minimize drying shrinkage.

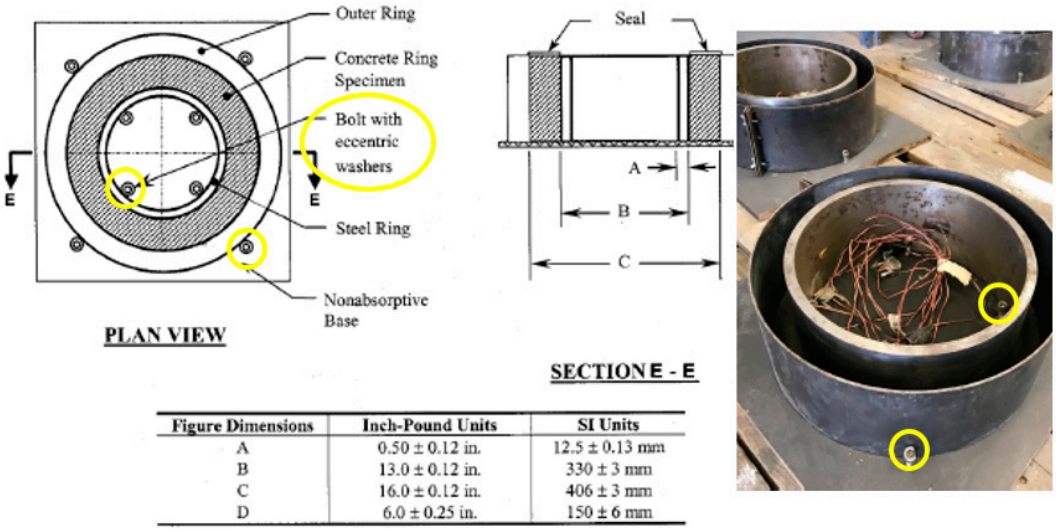

Figure Dimensions	Inch-Pound Units	SI Units
A	0.50 ± 0.12 in.	12.5 ± 0.13 mm
B	13.0 ± 0.12 in.	330 ± 3 mm
C	16.0 ± 0.12 in.	406 ± 3 mm
D	6.0 ± 0.25 in.	150 ± 6 mm

Figure 7. Schematic overview ring test (**left**) [17], actual setup ring test (**right**).

2.2.6. Autogenous Shrinkage Measured with Fiber Optic Sensors and Strain Gauges

To measure the shrinkage of the wall, fiber optic SOFO sensors (standard deformation sensor with a French acronymfor Surveillance d'Ouvrages par Fibres Optique from the company SMARTEC) based on low-coherence interferometry (Figure 8a,c,d)) were embedded in the walls before casting. The sensors were mounted on the steel reinforcement mesh at three positions: Bottom (B), middle (M) and top (T) at the height of 0.12 m, 0.705 m and 1.3 m, respectively, measured from the upper slab surface. In total five sensors were embedded in the wall: Three sensors with an active length of 1 m (T, M and B2) and two smaller sensors with an active length of 0.2 m at the bottom edges (B1 and B3) to monitor the autogenous shrinkage (AS) behavior of the edges.

SOFO sensors measured the real-time deformation inside the wall, whereas demountable mechanical strain gauges (DEMEC) measured the deformation on the exposed surface of the wall to see the effect of SAPs under drying conditions. DEMEC points were glued on the wall (after demolding) at three different levels: at the bottom at 0.12 m from the slab base, 10 points were glued with a 200 mm spacing between the points and the first and last point were positioned 100 mm away from the edges. Same goes for the ten middle points positioned at 0.7 m from the slab base and for the 10 top points at 1.3 m height, see Figure 8b,d. The DEMEC measurements were manually taken each day for two weeks, and then one measurement at two months and a last one at 120 days (4 months), which was the end of the testing period. In Figure 8d the positions of the SOFO sensors and the DEMEC points in and on the wall are depicted.

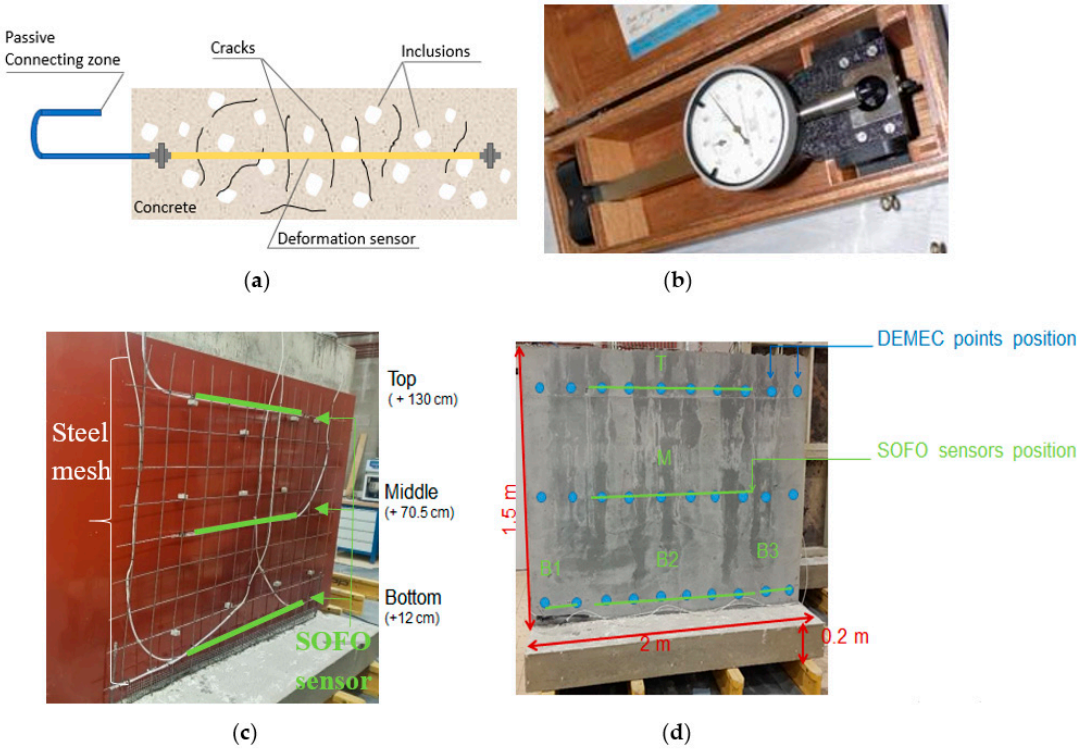

Figure 8. (**a**) Schematic diagram of the fiber optic sensor SOFO embedded in a concrete mixture [45]; (**b**) the strain gauge demountable mechanical strain gauge (DEMEC) used for measuring deformations manually; (**c**) steel mesh grid and SOFO positions; (**d**) accurate positions of the SOFO sensors and the DEMEC points for autogenous shrinkage (AS) measurements.

2.2.7. Water Flow

The ability of water to flow through the main crack formed in the REF wall (see later Section 3.3) was investigated by water flow tests using Karsten tubes and flow tests in which a basin was attached to the wall on the location of the crack. The basin, Figure 9a, was prepared using concrete plywood plates and sealed with waterproof glue to avoid water leakage. The basin has a height of 90 cm, an inner width of 21.5 cm and an inner depth of 10 cm. It was glued on the wall, and all edges and corners were sealed again. A thin layer of epoxy was added to the bottom of the basin in order to avoid water leaking through the connection wall-slab. The basin was filled with 14 liters of water two times on two consecutive days, and every hour (for 6 h) the level of water was recorded to see how much water was passing through the whole crack. The basin was then removed, and the reference wall was placed horizontally. Three Karsten tubes were positioned on the same crack within the reference wall but at positions with different crack widths, one at a crack width = 180 µm, one at 80 µm and one at around 40 µm, see Figure 9b. This method provides information on the amount of penetrating water per unit of time. The procedure was performed following the RILEM Test Method II.4 [46]: vertical tubes, with a capacity of 4 mL, were used; the total height of the water column applied amounted to 120 mm. The tubes were applied on the wall by interposing plasticine between the circular end of the tube and the flat surface of the wall, to ensure good adhesion manual pressure was exerted as well on the cylinder. Water was then slowly added to the tube through the upper opening, to avoid the accumulation of water bubbles, until it reached the zero-gradation mark. The amount of absorbed/permeated water was directly read from the graduated tube at a specific time. The water level was recorded at intervals of 1 min for the first 15 min, and then at intervals of 5 min for the remaining 45 min. The test was repeated four times at every location. The water penetration capacity is then obtained in mL per minute.

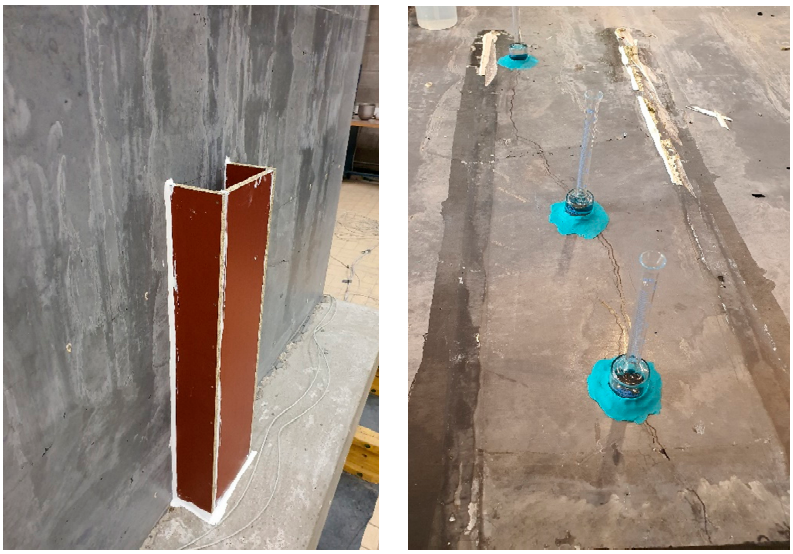

(**a**) (**b**)

Figure 9. (**a**) Water basin attached to the reference wall on the position of the longest crack, (**b**) three Karsten tubes placed on the longest crack of the reference wall at different crack widths.

3. Results

3.1. Hardened Properties of the Concrete Slabs

The 7-day strength and the 28-day strength of the slabs were 48.8 ± 0.7 MPa and 57.6 ± 2.2 MPa, respectively. At the latter age, the E-modulus was 39.6 ± 0.8 GPa.

3.2. Fresh and Hardened Properties of the Concrete Walls

The results of the slump flow test, air content and density measurements and the final setting time are summarized in Table 3. In the case of the SAP mixture, extra superplasticizer and water was added to compensate for lower workability, and thus, slump flow, due to the addition of the SAPs. The results show that the added amount of extra water and superplasticizer indeed resulted in the same workability as for the reference mixture without SAPs. The final setting time measured by penetrometer was 5.5 h for the REF mixture and 9 h for the SAP mixture. In the case of SAP addition, there is a delay in setting time, which is in accordance with earlier findings of the authors [31], and with findings reported in the literature [12,47,48].

Table 3. Fresh concrete properties for the reference mixture (REF) and the SAP mixture.

	REF	**SAP**
Slump flow [mm]	706 ± 22	698 ± 27
Air content [%]	2.7	2.5
Density [kg/m^3]	2400	2340
Final setting time [hrs]	5.5	9

The compressive strength and E-modulus for both the REF and the SAP mixtures are summarized in Figure 10 and Table 4. In Equation (1), f_{cm} was taken equal to the value obtained for the strength at 85 days for the REF and 63 days for SAP mixtures. In Equation (2), 28 was replaced by 85 for REF and 63 for SAP calculations and t by 28 to obtain the compressive strength values at 28 days. Theoretical compressive strength values are shown in light gray in Figure 10.

$$f_{ctm}(t) = \beta_{cc}(t) \cdot f_{cm}, \quad (1)$$

With

$$\beta_{cc}(t) = \exp\{s \cdot [1 - (\frac{28}{\frac{t}{t_1}})^{0.5}]\}, \quad (2)$$

where:

$f_{ctm}(t)$ mean compressive strength of concrete [MPa] at an age t [days]
f_{cm} mean compressive strength of concrete [MPa] at an age of 28 days
$\beta_{cc}(t)$ function to describe the development of compressive strength with time
t_1 = 1 day
t concrete age [days]
s coefficient which depends on the strength class of cement (taken here as 0.2)

Due to the formation of macro-pores upon shrinkage of the SAPs, the compressive strength in the case of the SAP mixture is lower compared to the reference mixture. After seven days, the compressive strength of the SAP mixture is 11% lower than the strength of the reference mix, and 11.5% at 28 days. The addition of SAPs did not have a significant influence on the E-modulus, at neither concrete age.

Table 4. E-modulus for the reference mixture (REF) and the SAP mixture.

	E-Modulus (Gpa)	
REF	7 days: 57 ± 15	85 days: 57 ± 13
SAP	7 days: 57 ± 3	63 days: 57 ± 8

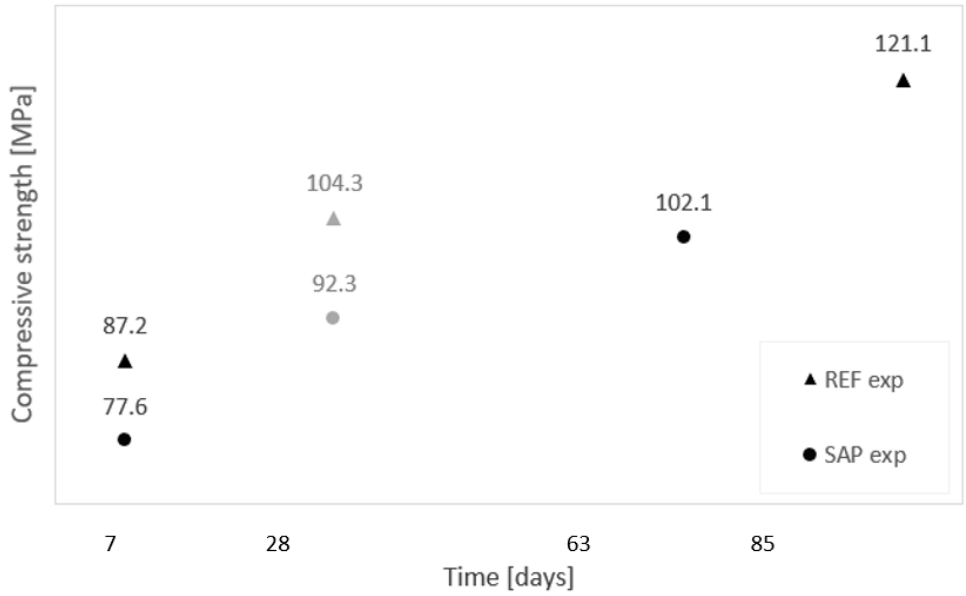

Figure 10. Compressive strength of the reference and the SAP mixtures determined experimentally. At 28 days, the values were modelled according to the strength evolution equation [40].

3.3. Crack Formation in the Walls

The first crack in the reference wall appeared at approximately 21 h after first contact mixing of water and cement (which corresponds to about 2 h after formwork removal), whereas the wall containing the SAPs did not present visible cracks until the end of the experiment. The cracks of the reference wall can be clearly seen in Figure 11. It should be noted that the longest crack passes through the whole section of the wall. At the bottom of the largest crack, the crack width was 180 µm (position a), halfway the crack height, the width was 80 µm (position b), and at the top of the crack, the width was only 40 µm (position c). All of the other cracks were non through-going cracks and had a maximum width of 50 µm.

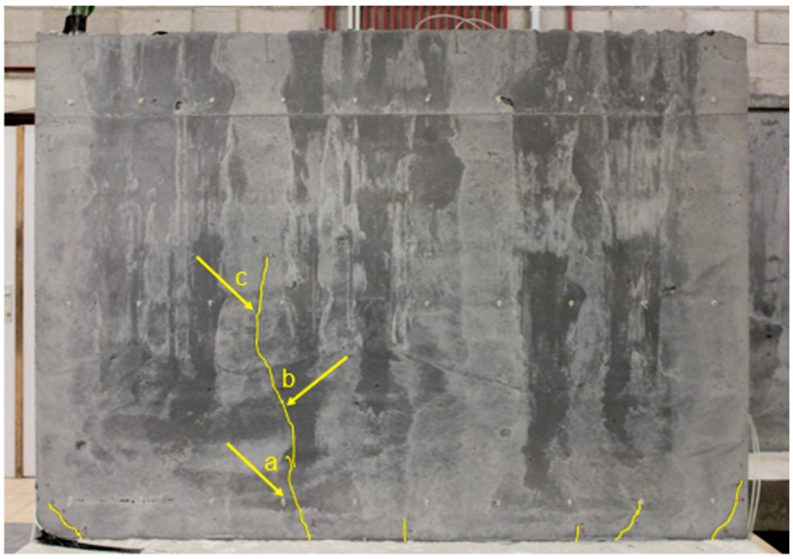

Figure 11. Crack formation in the reference wall. The cracks are indicated with yellow lines, and the letters a, b, c of the longest crack represent the locations where crack widths of 180 µm, 80 µm and 40 µm were measured, respectively.

3.4. Autogenous Shrinkage Measured with Corrugated Tubes

The results for the autogenous shrinkage measurements are plotted from the point of final setting, determined by the penetrometer test (see Figure 12), the zero point on the x-axis represents the time of the water−cement contact. For the reference mixture, the autogenous shrinkage strain after 20 days lies in the range of [−500, −610] µm/m, whereas for the SAP mixture the strain values lie in the range of [+50, +80] µm/m for the same time. The positive values in the case of the SAP mixture indicate that the mixture is expanding while the negative values for the reference mixture indicate shrinkage. From these results, it can be seen that the SAPs mitigate autogenous shrinkage very efficiently in this HPC mixture.

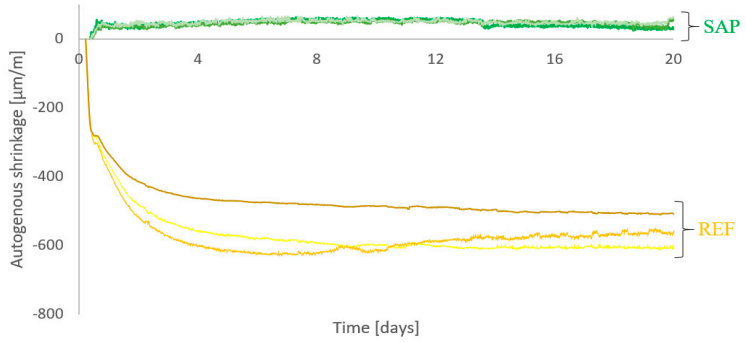

Figure 12. Autogenous shrinkage results of reference and SAP mixtures obtained from corrugated tubes plotted from the final setting time for the reference mixture (5.5 h), and the SAP mixtures (9 h).

3.5. Restrained Shrinkage: Ring Tests

Figure 13 shows the restrained shrinkage results that were followed up to 20 days. In the case of the REF samples, one of the strain gauges was not working properly. This is the reason, why there are only two strain measurements depicted in the graph. The REF samples (red curves) cracked after approximately two days (jump upwards in the strain), whereas the SAP samples (blue curves) showed no cracks along the whole period of measurement. During the first two days of measurement, the strain values of the REF samples were much higher (up to almost −120 µm/m) compared to the strain values of the SAP samples (maximum −10 µm/m).

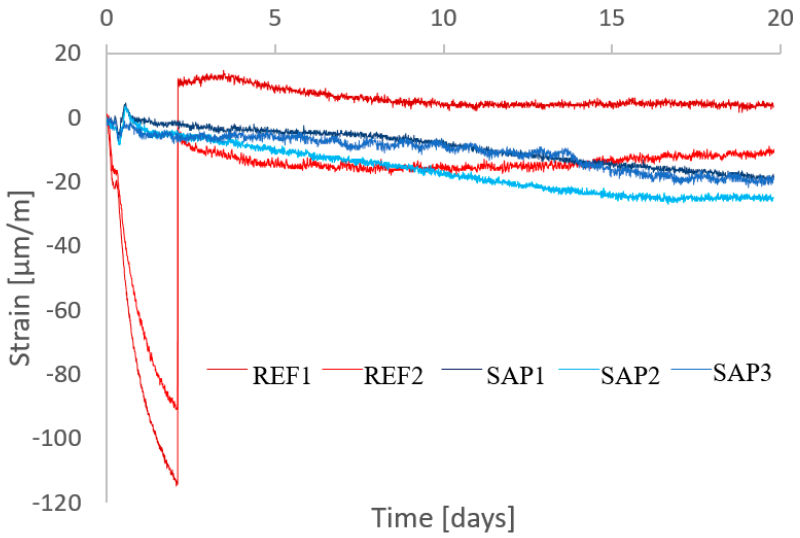

Figure 13. Restrained shrinkage results of the reference and the SAP mixtures using ring test method.

3.6. Autogenous Shrinkage Measured in the Wall with Fiber Optic SOFO Sensors and DEMEC Strain Gauges

The autogenous shrinkage curves represented in Figure 14 show the registered values taken from the long SOFO sensors (length 1 m). Measurements were recorded up to four months (120 days) to monitor the major part of occurring shrinkage deformations. The nomenclature in the figures goes as follows: The first part designates the walls either the reference (REF) or the one with SAPs, while the second part is reserved for the position of the fiber optic sensor as described in the materials and methods section.

In Figure 14a,b, the starting point of the measurements is plotted from the final setting time for the REF wall (5.5 h) and the SAP wall (9 h), the zero point on the figures corresponds to the first contact between the water and the cement. The shrinkage of the SAP wall remains significantly lower than the REF wall. The difference in the shrinkage behavior at different positions of the SOFO sensors can barely be noticed in the SAP wall; this could be an indication of the equal distribution of SAPs inside the wall, therefore, realizing a uniform internal curing behavior. On the other hand, for the REF wall, the increasing shrinkage from the bottom to the top clearly shows the restrained shrinkage condition at the bottom of the wall. A big difference can also be seen between the behavior of the bottom and the behavior of the middle and top sensor, the shrinkage difference between the top and the middle is around 200 µm/m, whereas the one between the middle and the bottom is around 400 µm/m. The shrinkage evolution of the bottom sensor (REF_B) was studied more into detail at the very early-age (0–24 h), and a change in the slope of the derivative curve was shown at around 19 h which was the time when the first crack was seen (19 h on the shrinkage curves of the sensors corresponds to 21 h because these sensors started measuring after 2 h of water-cement contact), see Figure 14c. This crack passed through the bottom sensor, thus at that moment of crack formation, there was a relaxation of the stresses that explains the lower values for the AS curve at the bottom along the whole measurement time. The early jump in the AS curves in Figure 14b is explained by the release of water from the SAPs. The released water acted as an internal water source for further hydration of the cement grains, thus reducing the capillary pressure inside pores known to induce autogenous shrinkage. This release also explains the big difference between the SAP shrinkage curves and the REF ones as discussed before. At 120 days, the AS was reduced by 22% at the bottom, 54% in the middle, and 60% at the top (Figure 14). The reduction of the shrinkage at the bottom cannot be really compared due to the crack formation and the relaxation of stresses around the sensor as discussed before. It is shown that AS was reduced at all levels in the SAP wall, which points out the positive effect of SAPs in HPC towards reducing autogenous shrinkage.

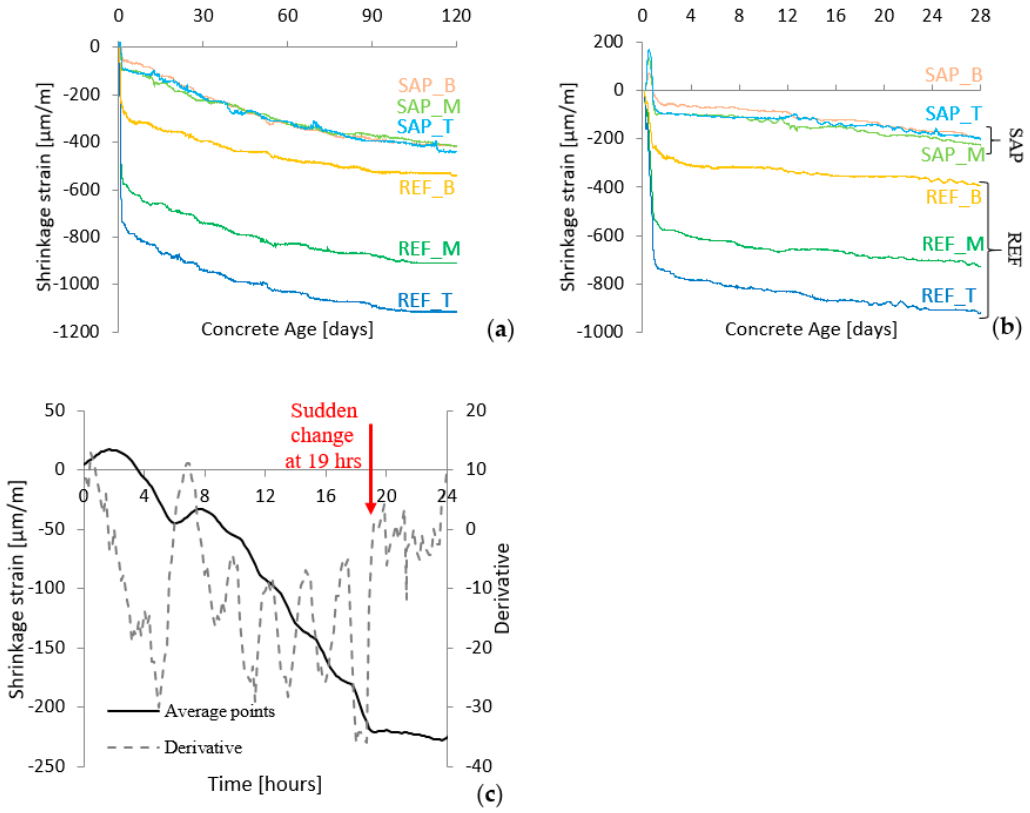

Figure 14. Autogenous shrinkage (AS) curves measured from the fiber optic sensors embedded in the reference and the SAP walls at three different levels: bottom, middle and top, (**a**) shrinkage curves represented for a period of 120 days for both walls, (**b**) shrinkage curves represented for 28 days and (**c**) is a representation of the early-age (24 h) of the derivative and the shrinkage curves of the bottom sensor of the reference wall.

Figure 15 shows the shrinkage curves representing the DEMEC measurements as the average of 10 measuring points glued on the wall at different levels: the bottom (a), the middle (b) and the top (c).

The zero point on the time axis corresponds to the water-cement contact, and the starting point of these curves is the start of the DEMEC measurements which is 23.5 h after casting for the reference wall and 24 h for the SAP wall. From Figure 15, it can be noticed that the DEMEC measurements confirm the observations made by the internal SOFO sensors: The deformations induced by shrinkage were much more pronounced in the reference wall than in the SAP wall. For these measurements, the values of the shrinkage at 120 days of both mixtures seem to be less than the one obtained by the embedded sensors—this is due to the fact that these curves starts at 24 h after water-cement contact where much shrinkage has already happened and was not taken into account. This shows how the SAPs highly reduce the shrinkage even when the surface is exposed to drying conditions. In HPC concrete, drying shrinkage is not considered to be of great significance, because the matrix is very dense. Nevertheless, drying might happen on the exposed surface of the SAP wall, where SAP particles are exposed to the outside so when they release their water, evaporation might be faster than water going into the matrix for further hydration of unhydrated cement grains. That might be an explanation of the lower shrinkage strain results obtained from DEMEC for the SAP wall when compared with the SOFOs.

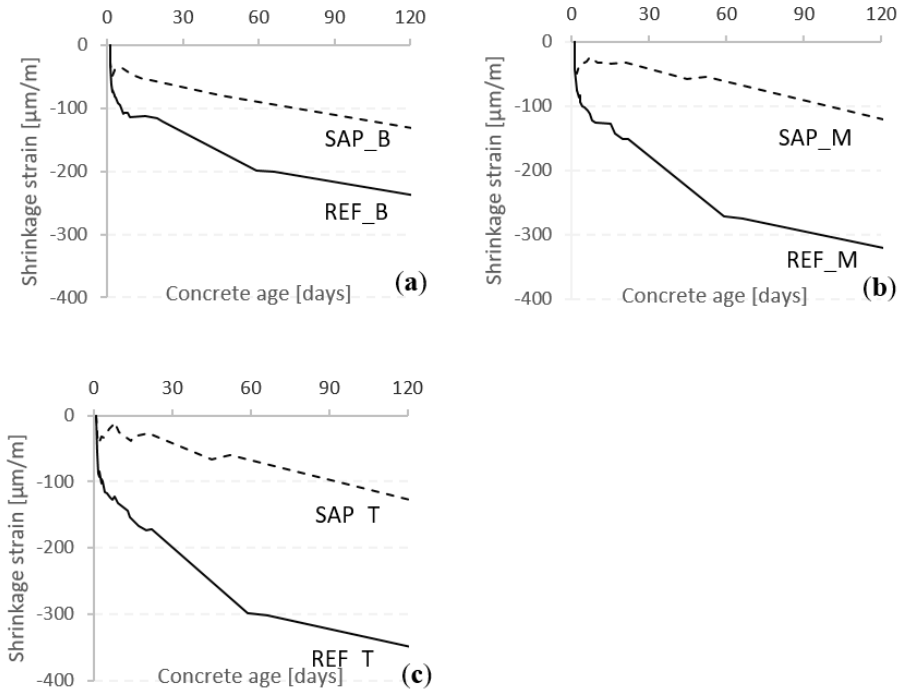

Figure 15. Shrinkage strain curves obtained from the demountable strain gauges measurements recorded manually: DEMEC curves are the average curves of 10 points for each position (**a**) bottom, (**b**) middle and (**c**) top; t_0 = time of water-cement contact; DEMEC measurements started 23.5 h after casting for the reference wall and 24 h for the SAP wall.

3.7. Water Flow

Water flow tests were performed to evaluate the flux of water penetrating the walls. A flow of around 1 L per hour was recorded resulting from two measurements performed over two consecutive days. The SAP wall had no visible cracks, so the test was only performed on the REF wall.

To further test the effect of the crack width on the flux of water, Karsten tubes were used. Values of these measurements are found in Figure 16. As can be seen, the flow is reduced gradually with the width of the crack. At 40 µm, the test was stopped after 1 h because the flow was still very low. The average flow of water was equal to 0.41 mL/min for the 180 µm, 0.23 mL/min for the 80 µm and 0.0075 mL/min for the 40 µm crack.

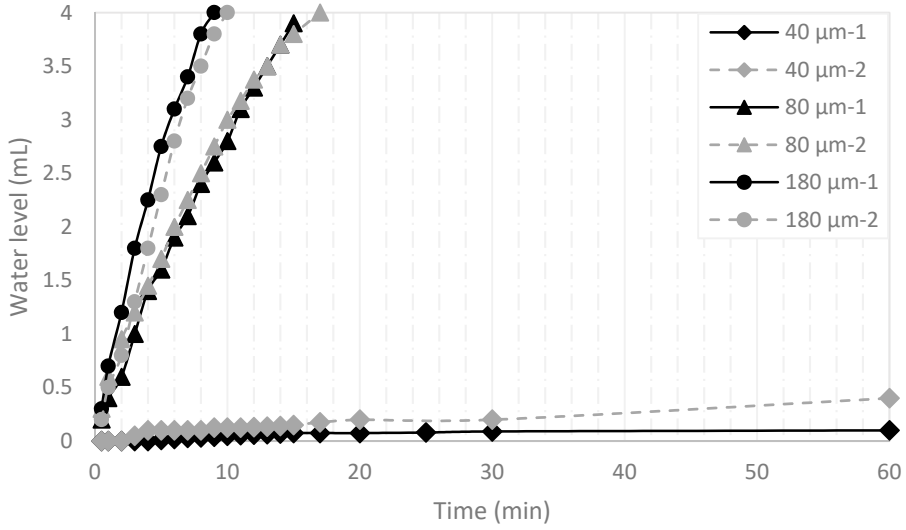

Figure 16. Karsten tubes results of water flow at different crack widths: 40 µm, 80 µm, and 180 µm.

4. Discussion

4.1. Fresh and Hardened Properties of the Walls

The fresh and hardened properties of both walls containing the reference and the SAP mixtures were studied. The range of the slump flow values lies within the class SF2, which is considered for wall construction according to the European guidelines for self-compacting concrete [49]. Slump flow of the SAP mixture was kept equal to the reference one by adding an extra amount of superplasticizer equal to 0.1 m% (by weight of cement). As SAPs tend to absorb a large amount of water from the mixture during the first hour, it will result in lower flowability and workability properties, even though the extra amount of water needed by SAPs is accounted for. Therefore, the addition of superplasticizer has helped in the repulsion of cement grains and SAPs in order to release the entrapped water for a better flowability of the mixture at the early-age stage.

The compressive strength of the studied mixtures falls into the category of high strength concrete with a grade of C100. A strength reduction of 11% at seven days and 11.5% at 28 days was seen for the SAP mixture versus the reference as expected, since these polymers release their water into the concrete after the skeleton has been already formed. With this release, a formation of macropores inside the matrix is created due to the volume reduction of SAPs.

The SAP blended concrete shows a lower strength, especially when additional water is used, which can be controlled and limited, given the targeted application and the chemistry of the SAP. However, the concept of durability should be discussed beyond strength itself. The concrete should not only present a certain required strength, but must also resist the effects of aggressive agents and environments during its service life. Tenorio Filho et al. [24] presented a SAP blended concrete with full mitigation of autogenous shrinkage and reduction of only 14% in the compressive strength at 28 days of age in comparison with a reference concrete with same effective water to cement ratio as the SAP blended concrete. When the comparison was made with another reference concrete containing the same total water to cement ratio as the SAP blended concrete, no reduction in compressive strength was noticed, but the SAP blended concrete was still able to completely mitigate the autogenous shrinkage. The same concrete compositions have been tested for salt scaling resistance under freeze-thaw cycles [50] where the SAP blended concrete showed a reduction of 50% in the scaled material after 28 cycles, in comparison to a reference concrete with the same effective water to cement ratio. It should be emphasized that the pores formed by SAP are closed, disconnected pores, which will affect the porosity, and hence, the strength, but less the permeability and durability since pore connectivity is an important factor here.

4.2. Restrained Shrinkage

The expansion perceived in the restrained deformation curves of the SAP specimens during the early days (Figure 13), is caused by the water released from the SAP particles at that time. In the REF wall, the cracks occurred around 21 h after water contact (see Section 3.3), whereas in the case of the ring test, the crack in the REF sample only appeared two days after water contact. This could be due to the fact that in the case of the rings, the samples were fully wrapped in plastic foil and a different geometry and restraining conditions are present between the rings and the walls. Nevertheless, these results confirm that the addition of SAPs can mitigate shrinkage and prevent cracking of HPC concrete.

4.3. Autogenous Shrinkage

Autogenous shrinkage results were represented through three different measurements techniques for the same concrete batches. Firstly, according to the standardized method by ASTM, the corrugated tubes filled with concrete were used; secondly, real-time shrinkage strains were measured automatically by fiber optic sensors embedded inside the walls and thirdly, shrinkage strains were measured manually using strain gauges (DEMEC). Results of these measurements are present in Sections 3.4 and 3.6. Under unrestrained and sealed conditions, SAPs completely mitigated the shrinkage, as seen in Figure 12.

It seems that the water released from these polymers was completely used for extra hydration of unhydrated cement grains, and thus, reduced the development of capillary tension inside the matrix. In the walls, the addition of SAPs did not completely reduce the AS, but it reduced the shrinkage strains to a high extent in comparison with the REF mixture. The difference between the standardized method and the real-time measurements could be due to the conditions and geometry differences between the two tests. In Figure 14, REF wall tends to reach a stable strain value at 90 days, which is earlier than for the SAP mixture because its water is lost first. Given the extra water provided by the SAPs over time, the effects of drying are delayed in comparison to the REF, and that could be the reason why there is still a tendency of increasing the shrinkage strain in the curves of the SAP wall. Shrinkage measurements from the short sensors B1 and B3 in Figure 8d with an active length of 200 mm were also investigated, it was found that the shrinkage values obtained from B1 were 23% lower than for B2 (long bottom sensor), and that is because the presence of many cracks at the edges. When a crack appears, there will be a relaxation of stresses in the zone around the crack. Therefore, sensors that overpass a crack will measure less strain deformations due to the relaxation of stresses that took place. Thus, sensor B1 measured less strain deformations than B2, given that B1 had more cracks over its smaller length. Measurements obtained from B3 were not taken into consideration since it represented a large amount of noise while analyzing its results.

The starting point of the shrinkage measurements is a very critical choice in order not to fall into an overestimation or an underestimation of the shrinkage. There is no consensus in the literature on which point to take as the beginning of the shrinkage measurements: t_0 is considered sometimes as the point of the initial or final setting time of the mixture, and some other times as the knee point (the point where the curves start to flatten) taken from the curves representing autogenous shrinkage [51–53]. In the rate of heat evolution method [54], time-zero is considered to be the point where the temperature rate curve of the studied concrete starts to increase sharply (initial setting time), and the peak of the temperature rate curve is considered the final setting time. If the time-zero is taken as the initial setting time, it will lead to an underestimation of the internal curing effect promoted by the SAPs and an overestimation of the shrinkage strain, and there is not so much difference in strains when choosing the knee point or the final setting time as shown by Filho et al. [51]. AS curves were presented in this study from the final setting time, but they were also further investigated by considering the knee point as time zero. Results obtained showed that the top of the reference wall, in this case, reached 410 μm/m of shrinkage strain at 120 days and 365 μm/m for the middle, while around 360 μm/m for the SAP wall was measured at all levels (there was no big difference between the SAP strain curves at the different levels). It should also be mentioned that when considering the apparent knee point from the shrinkage strain curves of the actual walls, it seems that the setting time happened at around 22 h of age for the REF wall and 24 h for the SAP wall (since the knee point is always close to the final setting time as demonstrated by Filho et al. [51]). However, if the rate of heat evolution is to be considered, then the peak in the temperature rate curve must be the setting time which in the case of the reference wall was at around 12.5 h based on simulation. In another study on the same reference mixture(own unpublished data), autogenous deformations were investigated through Free-Deformation (FD) system and the Temperature-Stress Testing Machine (TSTM) system. Shrinkage strain values obtained were around −700 μm/m (t_0 = 8 hrs) both under isothermal and realistic conditions at 10 days of age (with a temperature of 20 °C and a 30% of restraint degree), which corresponds reasonably well to the values obtained for the reference mixture under isothermal conditions in Figure 12 and under the realistic condition in Figure 14 at the same age. Therefore, in this case, considering the apparent knee point or the temperature rate curves resulted in an underestimation of the autogenous shrinkage and the approved solution was to choose the final setting time as the start of the autogenous shrinkage measurements.

4.4. Water Flow

Water flow tests were performed to evaluate the flux of water penetrating the walls. Permeability is indeed dependent on the crack width opening, the higher the crack width, the higher the water permeability and the lower the water-tightness [25].

There exists a relationship between the crack width w (m) and the flow rate q (m^3/s) for a through-depth crack as proposed by Edvardsen [55]:

$$q = \xi \frac{\Delta p \cdot b \cdot w^3}{12\eta \cdot \mathrm{d}}, \quad (3)$$

where ξ is a dimensionless reduction factor that takes into account the roughness of the crack walls and the deviation from a fully developed laminar flow, taken here equal to 0.17. The difference in pressure between the inlet and outlet is Δp expressed in N/m^2 with a value equal to 1176.5 that corresponds to a water head of 0.12 m. the crack length b (m) is taken here equal to the inner diameter of the Karsten tube being 0.025 m, η is the dynamic viscosity of the fluid (here water and equal to $1.002 * 10^{-3}$ Ns/m^2), and d is the distance that the fluid has to travel which is the thickness of the wall and equal to 0.05 m. Table 5 shows the measured and the calculated flow rates expressed in ml/min.

The difference between the measured and the calculated flow rates for the different crack widths confirms Edvardson's relation for the 80 µm and the 180 µm crack width, a higher difference percentage is registered for the lower 40 µm crack width. Van Mullem et al. [56] studied the variation of the results for the same crack width and concluded that for different specimens with a nearly identical crack width, a high variation on the flow rate can still exist, and at least six specimens should be taken into account for the calculation of the flow rate. When the test is executed on one specimen, the error can be the result of the small changes in the water head, the small particles which detach from the crack wall and either block a certain part of the crack or are flushed out, the small changes in the environmental conditions and/or the operator sensitivity. Thus, the higher difference found in Table 5 could be the result of all of these types of errors.

Table 5. Results of the measured and calculated flow rates passing the crack of the reference wall.

Flow Rate (mL/min)	**Crack Width**		
	40 µm	**80 µm**	**180 µm**
$\mathbf{q_{measured}}$	0.0075	0.23	0.41
$\mathbf{q_{calculated}}$	0.005	0.25	0.34
Difference (%)	33%	8%	17%

5. Conclusions

The behavior of SAPs towards mitigating the shrinkage in HPC wall elements was investigated in this study. Despite some minor difficulties in controlling the workability with SAPs and the slightly negative effect on the strength, the results show a promising scenario for the application of SAPs in real structures as it was demonstrated with these large-scale tests. The following conclusions can be drawn:

- The compressive strength of the SAP mix is 11% lower than the REF one at seven days and 11.5% at the later-age (28 days) due to the presence of the SAPs that become pores after the release of their water. Nevertheless, the compressive strength of the SAP mixture remains in the same class as the reference one, and the concrete is still classified as HPC.
- Autogenous shrinkage results for the SAP wall, clearly showed how the addition of SAP in concrete reduces the AS over a period of four months. This type of shrinkage was investigated using corrugated tubes filled with concrete, while real-time deformations were recorded using fiber optic SOFO sensors embedded in the walls and measurement points for mechanical strain gauges were placed on the wall. The early release of water from the SAPs into the matrix reduced

the shrinkage of the structure over the complete measurement period (up to 120 days of age). Thanks to the SAP incorporation, the shrinkage of the walls was reduced by 22% at the bottom, 54% in the middle, and 60% on top.

- Restrained shrinkage tests were also performed on concrete using ring tests to further understand the behavior of HPC toward restrained conditions. The specimens for the REF mixtures cracked after only two days, whereas SAP specimens didn't crack over the whole testing period (20 days).
- Cracks were shown on the reference wall at the early-age stage, after 21 h. The biggest crack reaches the middle of the wall and is 180 μm large at the bottom and 40 μm at mid-height of the wall. Over the four months of testing, no cracks were seen on the SAP wall.
- Water flow measurements were performed on the main crack of the reference wall, the water flow rate indeed increased with the third power of the crack width, as can be found in the existing literature.

Author Contributions: Conceptualization, L.D.M., J.K., K.V.T., N.D.B.; Methodology, L.D.M., J.K.; Formal analysis, L.D.M., J.K., J.R.T.F.; Investigation, L.D.M., J.K.; Supervision, K.V.T., N.D.B.; Writing—original draft preparation, L.D.M., J.K.; Writing—review and editing, J.K. All authors have read and agreed to the published version of the manuscript.

Funding: These results are part of a project that has received partial funding from the European Union's Horizon 2020 research and innovation programme under grant agreement N°685445—LORCENIS and partial funding from the Research Foundation Flanders (FWO Vlaanderen) under project No G.0A28.16.

Acknowledgments: The authors gratefully acknowledge the support and provision of materials from Dirk Qvaeschning and Sara Irico (Dyckerhoff GmbH), and the collaboration with Tor Arne Hammer (SINTEF) and Anja Klausen (NTNU Trondheim) for TSTM testing and modelling of the reference wall.

Conflicts of Interest: The authors declare no conflict of interest.

References

1. Schröfl, C.; Mechtcherine, V.; Gorges, M. Relation between the molecular structure and the efficiency of superabsorbent polymers (SAP) as concrete admixture to mitigate autogenous shrinkage. *Cem. Concr. Res.* **2012**, *42*, 865–873. [CrossRef]
2. Bentz, D.P.; Jensen, O.M.; Hansen, K.K.; Olesen, J.F.; Stang, H.; Haecker, C.J. Influence of Cement Particle-Size Distribution on Early Age Autogenous Strains and Stresses in Cement-Based Materials. *J. Am. Ceram. Soc.* **2001**, *84*, 129–135. [CrossRef]
3. Snoeck, D.; Jensen, O.M.; De Belie, N. The influence of superabsorbent polymers on the autogenous shrinkage properties of cement pastes with supplementary cementitious materials. *Cem. Concr. Res.* **2015**, *74*, 59–67. [CrossRef]
4. Kovler, K.; Zhutovsky, S. Overview and future trends of shrinkage research. *Mater. Struct. Constr.* **2006**, *39*, 827–847. [CrossRef]
5. Lura, P.; van Breugel, K.; Maruyama, I. Effect of curing temperature and type of cement on early-age shrinkage of high-performance concrete. *Cem. Concr. Res.* **2001**, *31*, 1867–1872. [CrossRef]
6. Holt, E. Contribution of mixture design to chemical and autogenous shrinkage of concrete at early ages. *Cem. Concr. Res.* **2005**. [CrossRef]
7. Wu, L.; Farzadnia, N.; Shi, C.; Zhang, Z.; Wang, H. Autogenous shrinkage of high performance concrete: A review. *Constr. Build. Mater.* **2017**, *149*. [CrossRef]
8. Holt, E.E. *Early Age Autogenous Shrinkage of Concrete*; VTT Technical Research Center of Finland: Espoo, Finland, 2001; pp. 2–184.
9. Mechtcherine, V.; Reinhardt, H.W. *STAR 225-SAP Application of Superabsorbent Polymers (SAP) in Concrete Construction*; Springer Netherlands: Heidelberg, Germany, 2012.
10. Justs, J.; Wyrzykowski, M.; Bajare, D.; Lura, P. Cement and Concrete Research Internal curing by superabsorbent polymers in ultra-high performance concrete. *Cem. Concr. Res.* **2015**, *76*, 82–90. [CrossRef]
11. Jensen, O.M.; Hansen, P.F. Water-entrained cement-based materials I. Principles and theoretical background. *Cem. Concr. Res.* **2001**, *31*, 647–654. [CrossRef]

12. Piérard, J.; Pollet, V.; Cauberg, N. Mitigating autogenous shrinkage in HPC by internal curing using superabsorbent polymers. In Proceedings of the International RILEM Conference Volume Changes Hardening Concrete: Testing Mitigation, Lyngby, Denmark, 20–23 August 2006; pp. 97–106. [CrossRef]
13. Craeye, B.; Geirnaert, M.; de Schutter, G. Super absorbing polymers as an internal curing agent for mitigation of early-age cracking of high-performance concrete bridge decks. *Constr. Build. Mater.* **2011**, *25*, 1–13. [CrossRef]
14. Igarashi, S.; Watanabe, A.; Jensen, O.M.; Lura, P.; Kovler, K. Experimental study on prevention of autogenous deformation by internal curing using super-absorbent polymer particles. In Proceedings of the International RILEM Conference Volume Changes Hardening Concrete: Testing Mitigation, Lyngby, Denmark, 20–23 August 2006; pp. 77–86. [CrossRef]
15. Mechtcherine, V.; Gorges, M.; Schroefl, C.; Assmann, A.; Brameshuber, W.; Ribeiro, A.B.; Cusson, D.; Custódio, J.; da Silva, E.F.; Ichimiya, K. Effect of internal curing by using superabsorbent polymers (SAP) on autogenous shrinkage and other properties of a high-performance fine-grained concrete: Results of a RILEM round-robin test. *Mater. Struct.* **2013**, *47*, 541–562. [CrossRef]
16. Benboudjema, F.; Delsaute, B.; Honorio, T. *Thermal Cracking of Massive Concrete Structures*; Springer Cham: New York, NY, USA, 2019.
17. ASTM International. *ASTM C 1581-04, Standard Test Method for Determining Age at Cracking and Induced Tensile Stress Characteristics of Mortar and Concrete under Restrained Shrinkage*; American Society for Testing and Materials: West Conshohocken, PA, USA, 2004.
18. ASTM C1698-09. *Standard Test Method for Autogenous Strain of Cement Paste and Mortar*; American Society for Testing and Materials: West Conshohocken, PA, USA, 2010. [CrossRef]
19. Wong, A.C.L.; Childs, P.A.; Berndt, R.; Macken, T.; Peng, G.D.; Gowripalan, N. Simultaneous measurement of shrinkage and temperature of reactive powder concrete at early-age using fibre Bragg grating sensors. *Cem. Concr. Compos.* **2007**. [CrossRef]
20. Glišić, B. Fibre Optic Sensors and Behaviour in Concrete At Early Age. Ph.D thesis, Ecole Polytechnique Federale de Lausanne, Lausanne, Switzerland, 2000.
21. Glišić, B.; Simon, N. Monitoring of concrete at very early age using stiff SOFO sensor. *Cem. Concr. Compos.* **2000**, *22*, 115–119. [CrossRef]
22. Kristiawan, S.A.; Aditya, M.T.M. Effect of high volume fly ash on shrinkage of self-compacting concrete. *Procedia Eng.* **2015**, *125*, 705–712. [CrossRef]
23. Zdanowicz, K.; Marx, S. Shrinkage and Expansion Strains in Self-compacting Concrete: Comparison of Methods of Measurements. In *High Tech Concrete: Where Technology and Engineering Meet*; Springer Cham: New York, NY, USA, 2018; pp. 524–532.
24. Filho, J.R.T.; Mannekens, E.; van Tittelboom, K.; Snoeck, D.; De Belie, N. Assessment of the potential of superabsorbent polymers as internal curing agents in concrete by means of optical fiber sensors. *Constr. Build. Mater.* **2020**, *238*, 1–8. [CrossRef]
25. Wang, K.; Jansen, D.C.; Shah, S.P.; Karr, A.F. Permeability study of cracked concrete. *Cem. Concr. Res.* **1997**, *27*, 381–393. [CrossRef]
26. Cusson, D.; Hoogeveen, T. An experimental approach for the analysis of early-age behaviour of high-performance concrete structures under restrained shrinkage. *Cem. Concr. Res.* **2007**, *37*, 200–209. [CrossRef]
27. Recommendation of RILEM TC 260-RSC: Testing sorption by superabsorbent polymers (SAP) prior to implementation in cement-based materials. *Mater. Struct.* **2018**, *8*. [CrossRef]
28. Zhu, Q.; Barney, C.W.; Erk, K.A. Effect of ionic crosslinking on the swelling and mechanical response of model superabsorbent polymer hydrogels for internally cured concrete. *Mater. Struct.* **2014**, *48*, 2261–2276. [CrossRef]
29. Snoeck, D.; De Belie, N. Repeated Autogenous Healing in Strain-Hardening Cementitious Composits by Using Superabsorbent Polymers. *J. Mater. Civ. Eng.* **2013**, *25*, 864–870.
30. Schröfl, C.; Snoeck, D.; Mechtcherine, V. A review of characterization methods for superabsorbent polymer (SAP) samples to be used in cement-based construction materials: Report of the RILEM TC-260-RSC. *Mater. Struct. Constr.* **2017**, *50*, 197. [CrossRef]

31. De Meyst, L.; Mannekens, E.; de Araujo, M.A.P.G.; Snoeck, D.; van Tittelboom, K.; van Vlierberghe, S.; De Belie, N. Parameter Study of Superabsorbent Polymers for Use in Durable Concrete Structures. *Materials* **2019**, *12*, 1541. [CrossRef] [PubMed]
32. Wyrzykowski, M.; Lura, P.; Pesavento, F.; Gawin, D. Modeling of Water Migration during Internal Curing with Superabsorbent Polymers. *J. Mater. Civ. Eng.* **2012**, *24*, 1006–1016. [CrossRef]
33. Filho, J.R.T.; Snoeck, D.; De Belie, N. Mixing protocols for plant-scale production of concrete with superabsorbent polymers. *Struct. Concr.* **2020**, 1–9. [CrossRef]
34. Belgian Standard. *NBN EN 12390-3: 2019 Testing Hardened Concrete—Part 3: Compressive Strength of Test Specimens*; NBN, Bureau voor Normalisatie: Brussels, Belgium, 2019.
35. Belgian Standard. *NBN EN 12390-13: Beproeving van Verhard Beton—Deel 13: Bepaling van de Secans Elasticiteitsmodulus Bij Druk*; NBN, Bureau voor Normalisatie: Brussels, Belgium, 2005; p. 149.
36. Belgian Standard. *NBN EN 12350-8: Testing Fresh Concrete—Part 8: Self-Compacting Concrete Slump-Flow Test*; NBN, Bureau voor Normalisatie: Brussels, Belgium, 2019.
37. Belgian Standard. *NBN EN 12350-7: Testing Fresh Concrete—Part 7: Air Content Pressure Methods*; NBN, Bureau voor Normalisatie: Brussels, Belgium, 2019.
38. Belgian Standard. *NBN EN 12350-6: Testing fresh concrete—Part 6: Density*; NBN, Bureau voor Normalisatie: Brussels, Belgium, 2019.
39. Astm C403/C403M-99. Standard Test Method for Time of Setting of Concrete Mixtures by Penetration Resistance. *Annu. B ASTM Stand.* **1999**, *4*, 1–6.
40. Müller, H.; Aïtcin, P.C.; Bentur, A.; Chiorino, M.A.; Clement, J.L.; Curbach, M.; Faust, T.; Hammer, T.A.; Jaccoud, J.P.; Kessler-Kramer, C.; et al. *Constitutive Modelling of High Strength/High Performance Concrete*; International Federation for Structural Concrete: Lausanne, Switzerland, 2008.
41. Geiker, M.; Bentz, D.; Jensen, O. Mitigating autogenous shrinkage by internal curing. *ACI Spec. Publ.* **2004**, *218*, 143–148.
42. Jensen, O.M.; Hansen, P.F. Water-entrained cement-based materials II. Experimental observation. *Cem. Concr. Res.* **2001**. [CrossRef]
43. Lura, P.; Durand, F.; Jensen, O.M. Autogenous strain of cement pastes with superabsorbent polymers. In Proceedings of the International RILEM Conference Volume Changes Hardening Concrete: Testing Mitigation, Lyngby, Denmark, 20–23 August 2006; pp. 57–66. [CrossRef]
44. Ji, T.; Zheng, D.D.; Chen, X.F.; Lin, X.J.; Wu, H.C. Effect of prewetting degree of ceramsite on the early-age autogenous shrinkage of lightweight aggregate concrete. *Constr. Build. Mater.* **2015**, *98*, 102–111. [CrossRef]
45. SMARTEC. Standard SOFO Deformation Sensor, Guidelines and Installation Instructions, Manno, Switzerland. Available online: https://smartec.ch/wp-content/uploads/sites/2/2017/01/SOFO-Standard-Deformation-Sensor-E10-1010-SMA.pdf (accessed on 8 June 2020).
46. RILEM TC 25-PEM. *Recommended Tests to Measure the Deterioration of Stone and to Assess the Effectiveness of Treatment Methods, Materials and Structures*; RILEM Publications SARL: Paris, France, 1980; p. 75.
47. Rizwan, S.A.; Mustafa, S.; Ahmed, W. Mitigation of Early Age Shrinkage in self-Consolidating Paste Systems Using Superabsorbent. In Proceedings of the Materials, System and Structures in Civil Engineering (MSSCE-2016), Denmark Technical University, Lyngby, Denmark, 15–29 August 2016; pp. 443–453.
48. Dudziak, L.; Mechtcherine, V. Deliberations on Kinetics of Internal Curing Water Migration and Consumption Based on Experimental Studies on SAP-Enriched UHPC. In Proceedings of the International RILEM Conference on Use of Superabsorbent Polymers and other New Additives in Concrete, Lyngby, Denmark, 14–18 August 2010.
49. EFNARC. *"The European Guidelines for Self-Compacting Concrete: Specification, Production and Use"*. Available online: http://www.efnarc.org/pdf/SandGforSCC.PDF (accessed on 20 February 2002).
50. Filho, J.R.T.; Mannekens, E.; Snoeck, D.; De Belie, N. Salt-Scaling Resistance of SAP-Modified Concrete under Freeze-Thaw Cycles. In Proceedings of the 3rd RILEM Spring Convention 2020, Guimaraes, Portugal, 10–14 March 2020.
51. Filho, J.R.T.; de Araújo, M.A.P.G.; Snoeck, D.; De Belie, N. Discussing different approaches for the time-zero as start for autogenous shrinkage in cement pastes containing superabsorbent polymers. *Materials* **2019**, *12*, 2962. [CrossRef]

52. Hammer, T.A. Testing of Autogenous Deformation (AD) and Thermal Dilation (TD) of Early Age Mortar and Concrete—Recommended Test Procedure. In Proceedings of the International RILEM Conference on Volume Changes of Hardening Concrete: Testing and Mitigation, Lyngby, Denmark, 20–23 August 2006; pp. 341–346. [CrossRef]
53. Lyu, Y. Autogenous Shrinkage of Cement-Based Materials: From the Fundamental Role of Self-Desiccation to Mitigation Strategies Based on Alternative Materials. Ph.D thesis, Ghent University, Ghent, Belgium, 2018.
54. Mindess, S.; Young, J.F. *Concrete*; Prentice-Hall: Englewood Cliffs, NJ, USA, 1981.
55. Edvardsen, C. Water permeability and autogenous healing of cracks in concrete. *ACI Mater. J.* **1999**, *96*, 448–454. [CrossRef]
56. Van Mullem, T.; Gruyaert, E.; Debbaut, B.; Caspeele, R.; De Belie, N. Novel active crack width control technique to reduce the variation on water permeability results for self-healing concrete. *Constr. Build. Mater.* **2019**, *203*, 541–551. [CrossRef]